

Performance Comparisons on Fully-Actuated Multirotors with Different Actuation Modes

Caleb Probine, and Karl A. Stol*

University of Auckland, Department of Mechanical and Mechatronics Engineering, Auckland 1010, New Zealand

ABSTRACT

For the interaction of Unmanned Aerial Vehicles (UAVs) with the environment, their ability to station-keep is critical. In conventional station keeping, a UAV will change attitude to translate, and reject disturbances. Meanwhile, a fully-actuated UAV can exert these forces without rolling or pitching: this is also known as vectored thrust. These two methods of position control represent two actuation modes, with very different dynamics. The work presented in this paper investigates how Proportional-Integral-Derivative (PID) controllers can be tuned to compare the two actuation modes discussed in wind disturbance rejection tasks. The comparison is made fair by ensuring that actuator usage is the same between the two cases. Overall, when tuned for moderate control precision, it is found that the actuator usage is significantly higher when vectored thrust is used, making it less favourable for general station keeping tasks. However, linear model studies indicate that higher precision may necessitate the use of vectored thrust, rather than conventional methods.

1 INTRODUCTION

Given their numerous possible applications, such as agricultural assessments [1], traffic estimation [2], and power line inspection [3], UAVs have been increasing in their civil applications in recent years [4]. Within the range of different craft configurations, multirotors are particularly favourable for their ability to hover in place. Another unique capability of multirotors is their ability to interact with the environment, an example of which is given in [5]. In these environmental interaction tasks, a range of control issues exist such as the requirement to handle contact forces, and reject wind disturbances effectively.

Within the realm of multirotors, the class of over-actuated/fully-actuated crafts are of particular interest in these applications. These have the property of being able to generate a full 6-DoF wrench vector, and as a result, can regulate position and orientation independently. This is in contrast to

under-actuated crafts, which must roll or pitch to translate in the horizontal plane: the more conventional form of actuation. This wrench generation capability is a critical craft-capability for the handling of tools in the environment without external manipulators. Two common methods for achieving this full-actuation include the introduction of tilting rotors such as in [6], or the use of fixed-tilt rotors, such as in [7].

Whilst fully-actuated crafts must be used to allow full-pose tracking, there are various trade-offs when compared to under-actuated crafts. One of the core disadvantages of fully-actuated crafts are their lower efficiency, and this is documented well in a range of works. For example, in [8], the wastage of internal forces in fully-actuated crafts is articulated with a force efficiency index. A more dynamic observation of the inefficiency can be observed in [9]. In this work, for a fully-actuated craft, the frequency response of motor speeds to translation commands is compared for conventional actuation, and vectored thrust (translating without attitude-change). The latter, fully-actuated method of translation is found to result in higher rotor speeds at almost all frequencies. In [10], a craft that can transform between co-planar (under-actuated) and omni-directional modes is presented. Via a common mission, it is then shown that the energy usage when undertaking pure fully-actuated omni-directional flight is higher than that when the craft is converted between co-planar and fully-actuated modes as appropriate. However, a critical advantage in fully-actuated crafts is the faster response to forces. This is documented in the context of disturbance rejection in [11], and is experimentally verified.

Throughout works that present new crafts and control methods, the performance under the unique pose-tracking capability is frequently demonstrated: for example the work in [12] clearly showcases the omni-directionality of the new craft. However it is also of interest to benchmark the performance of fully-actuated UAVs against their under-actuated counterparts in common tasks. Some works that have addressed this are described below.

In [13], a tilting-rotors craft is described, and made to follow a trajectory under a wind disturbance. This experiment is undertaken in both 'conventional' and 'tilt-augmented' configurations, with the former being generated by locking the rotor tilting mechanism. Under identical control gains, poorer performance (higher overshoot) is observed with the tilt-augmented configuration. This method of making comparisons by changing the actuation modes used by the craft is far better than the alternative of comparing different crafts. A

*Email address: k.stol@auckland.ac.nz

similar approach has also been undertaken in [6, 14, 15].

In the comparisons presented in [6], mean absolute and standard deviation of position are used as comparison metrics in a common step tracking task, and similar performance is observed between the platforms. However, the comparison's validity is limited by vagueness in the controller tuning processes. Meanwhile, the authors of [14] tune controllers for each craft configuration with similar step responses, following which, their (sinusoidal) disturbance rejection performance is compared, showing an advantage for fully-actuated crafts. Finally, the authors of [15] compare tethered conventional and tilting rotors quad-copters under atmospheric wind disturbances. In this case, root mean square (RMS) position error is used to quantify position, with an advantage demonstrated for the tilting-rotors craft. Whilst these works present a range of useful metrics for assessing position tracking performance when comparing under-actuated and fully-actuated crafts, disparate conclusions are reached about their relative performance. This is due to inconsistent, rigor-limited tuning of the controllers.

Work that does approach closed-loop comparisons appropriately is presented in [16]. This work takes the approach of using non-linear dynamic inversion, to ensure that the position response between 3 multirotor configurations, is identical. Within these configurations both under-actuated and fully-actuated craft are included. In simple polynomial trajectory tracking simulations the actuator usage of these crafts is then compared, and the fully-actuated craft is shown to require higher actuator inputs to follow the trajectory. This consideration of position tracking and actuator usage makes for a highly rigorous comparison, however it is limited by the simplicity of the model used, which don't reflect aerodynamic effects, or motor models. It is also limited by the simplicity of the trajectory used.

In comparing actuator usage a range of metrics exist. In the context of optimising attitude controllers, the weighted \mathcal{H}_∞ norm of the actuator usage is constrained in [17]. Meanwhile, in position control optimisation for wind-rejection in [9], the \mathcal{H}_∞ norm of control input is added to the weighting when designing a controller. In simulation, different metrics are then used again. For example, in [18], Integral absolute input is used as a measure of force variation. Meanwhile, [9] analyses standard deviation in each motor's pulse-width-modulation (PWM) when assessing actuator usage.

In terms of the control techniques used on fully-actuated crafts, a range of advanced control schemes have been implemented, including sliding mode control [19], model predictive control [20] and adaptive control [21] among others. However, in [6, 15, 13], also observed was the use of simple PID and PD components within the control systems. Overall, PID controllers are useful for their simplicity and robustness, and they provide a good starting point for analysing craft control performance. A number of additional works have used simple controllers, often related to PID, with examples in-

cluding [10, 22, 23]. In some cases, lower level loops are augmented by feedback-linearised or geometric components, such as in [12].

Overall, this work aims to contribute to more rigorous comparisons of fully-actuated crafts in the context of disturbance rejection. In particular, PID tuning will be used as a basis to investigate the relative efficiency on a craft that is tuned to have similar performance in its fully-actuated and under-actuated modes.

The remainder of this paper is structured as follows. Section 2 gives a brief outline of the craft used in the comparisons undertaken. Section 3 then details the model of said craft is constructed. In addition, the methodologies for fair tuning comparisons are also presented. Section 4 then provides the results of these studies, after which Section 5 provides analyses of how the results change when the aggressivity of control changes.

2 MULTIROTOR DESCRIPTION AND ACTUATION MODES

The craft used as a basis for this comparison is shown in Figure 1. It has a flying mass of 1.72 kg and a rotor-to-rotor diameter of 500 mm . It was constructed, and modelled in [9], based on optimisation algorithms outlined in [24]. This craft is technically over-actuated, as it has 2 more motors than required for full actuation, however, as the redundancy is not a core point in this work, it shall be referred to it as fully-actuated. When discussing the craft, there are two frames of concern. Vectors in the fixed world frame are denoted with $^{\mathcal{W}}$. Meanwhile, $^{\mathcal{B}}$ is used to denote the body frame, which moves with, and is attached to, the craft.

Like an under-actuated craft, the octorotor can create lateral forces by rolling/pitching, which will be denoted as attitude-based thrust $^{\mathcal{W}}F_A$. However, given its full-actuation, it can also create lateral forces whilst keeping level, which will be denoted vectored thrust $^{\mathcal{W}}F_V$. These two actuation methods are depicted in Figure 2. Throughout the remainder of this paper, the subscript \cdot_A corresponds to attitude-based thrust control, whilst \cdot_V corresponds to vectored thrust control. When controlling position via vectored thrust, the command will always be commanded to stay level, which is



Figure 1: Craft for which control is tuned [9].

impossible with attitude-based thrust. Also note that when attitude-based thrust is utilised, comparisons will still be made using the canted craft: i.e. the craft will remain fully-actuated, but vectored thrust will not be used.

The control software used is the PX4 flight stack, which provides the framework in which control structures are encoded. The outer loops of this control structure are indicated in Figure 3, whilst the inner loops are described in Figure 4. The feedback supplied to the controller in Figure 3 is the position vector $\xi \in \mathbf{R}^3$, which has components as follows: $[\mathcal{W}x \ \mathcal{W}y \ \mathcal{W}z]^\top$. This control must be completed in the presence of wind disturbances $\mathcal{W}\mathbf{w}$, which have components in 3 axes. Also of concern is the actuator usage, as encoded by the 8 element vector χ , of the PWM motor commands.

At the highest level, a cascaded controller is used for each axis independently. This cascaded structure has position and speed loops for each axis, with the position loop being P controlled, and the velocity loop being PID controlled. This generates the translational commands for the craft.

For attitude-based thrusts, the translational commands are converted to angle set-points, which are in turn passed to a lower level attitude controller. This is again of a cascade structure, with angle and angle-rate loops respectively. For the angle loop, non-linear P control is used, whilst for the angle-rate loop, PID control is used for each axis. The output of this stage is a set of torques for the craft. Meanwhile, when vectored thrust is used, the desired forces are generated directly. In this case the attitude controller runs in parallel to the position controller, with constant zero references for orientation.

The lowest level component of this is a multirotor mixer: this converts from a vector of force and torque commands to individual motor commands.

3 MODELLING

3.1 Nonlinear Numerical Model

The control assessment methods all use the non-linear octocopter model defined in [9]. This details critical dynamics such as the drone's rigid body motion, a first-order non-linear motor model, alongside an empirical aerodynamic model. These physical control components are then accompanied by components representing the lower layers of the PX4 control architecture. These include a multirotor mixer, an attitude controller, and a conversion from attitude-based thrust commands to angle set-points. Links between these are all shown in Figure 4. This figure also demarcates the inputs and outputs of the plant.

When using attitude-based thrust control, the vector $\mathcal{W}F_A$ will be the control input, and $\mathcal{B}F_V$ will be zeroed. When using vectored thrust control, the vector $\mathcal{B}F_V$ will be manipulated, along with $\mathcal{W}F_{A,z}$. Because the craft is level during vectored thrust control $\mathcal{W}F_V = \mathcal{B}F_V$.

When the loop is closed, the focus is then on the closed-loop plant shown in Figure 3. Note that in this closed-loop

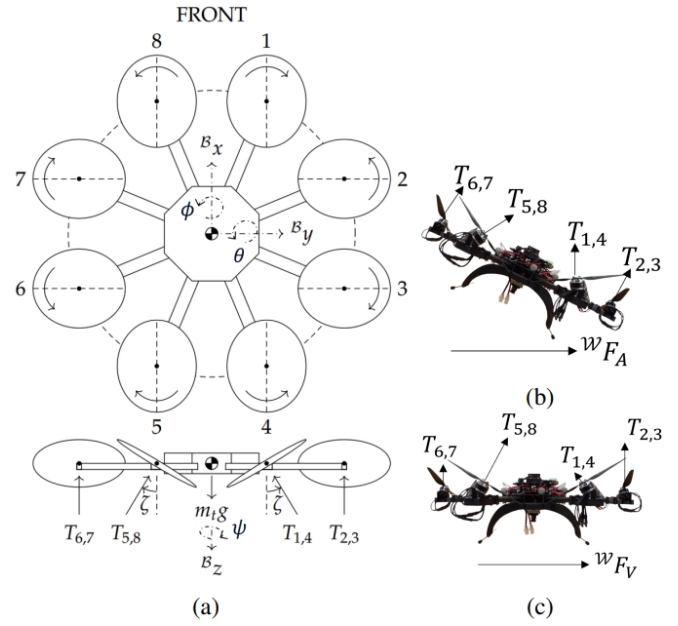


Figure 2: Craft dynamics illustrations. (a) Octocopter Schematic [9]; (b) Motor usage when translating with attitude-based thrust $\mathcal{W}F_A$ in the $\mathcal{W}y$ direction; (c) Motor usage when translating with vectored thrust $\mathcal{W}F_V$ in the $\mathcal{W}y$ direction [25]

plant, the reference is zero, and the response of the outputs to a random wind is of interest.

3.2 Linearisation Description

In order to convert the non-linear model to a linear one for analysis, Jacobian linearisation is undertaken. This requires the generation of an operating point about which to linearise, which is found via trim analysis. For trim analysis, the following constraint is applied on the wind

$$\mathcal{W}\mathbf{w}^* = [5.6 \ 0 \ 0]$$

This wind speed is chosen based on values used in [9]. Depending on the actuation method used, a second constraint is applied. When attitude-based is used,

$$\mathbf{u}^* = [\mathcal{W}F_{A,x} \ \mathcal{W}F_{A,y} \ \mathcal{W}F_{A,z} \ 0 \ 0]$$

is applied. Meanwhile, when vectored thrust is used,

$$\mathbf{u}^* = [0 \ 0 \ \mathcal{W}F_{A,z} \ \mathcal{B}F_{V,x} \ \mathcal{B}F_{V,y}]$$

is applied. It should be noted that in the linearisation process, the attitude control gains are fixed. Also, at this stage, the attitude controller model used is continuous. After MATLAB is used to solve for the entire trim point, the linear model can be generated.

3.3 Controller Tuning Methods

For tuning, existing gains are taken for attitude-based thrust control. These gains correspond to moderate preci-

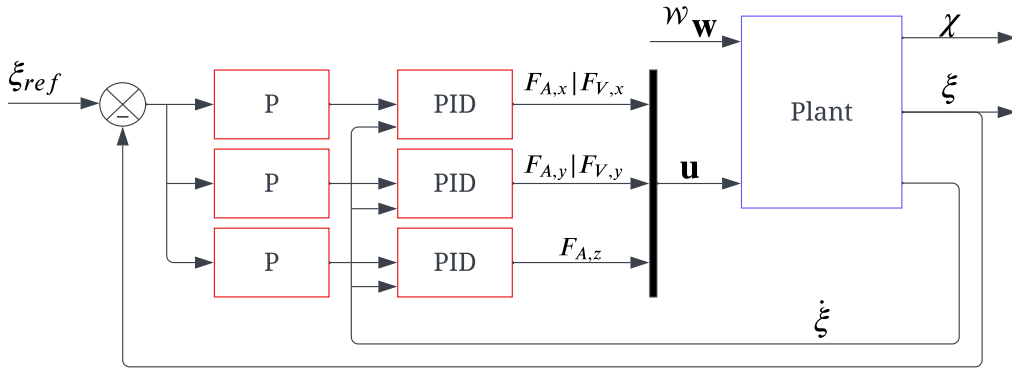


Figure 3: Control structure used in this work. Note that one pair of P-PID controllers exist for each axis. The gains for the first two axes are the same, whilst the W_z axis is different. Also note, depending on the actuation method being used, the W_x and W_y control actions will be mapped to different plant inputs. Finally, note that in the derivative components of the second loop, reference derivatives are not used.

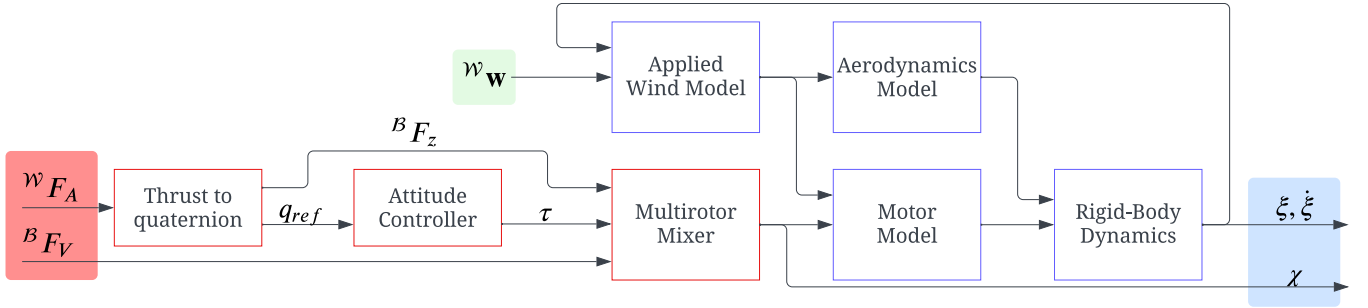


Figure 4: Components comprising the non-linear craft model. Red, green and blue regions respectively denote inputs, disturbance inputs and outputs of the model. Blue-outlined blocks represent physical model elements, whilst red-outlined blocks denote software elements. Note also that attitude feedback amongst these blocks is omitted for clarity.

sion, where there is still significant headroom for the actuators. These are given in Table 1. By closing the loop with attitude-based thrust control, and these gains, a linear model of the closed-loop process is generated. The linear model for attitude-based thrust control is then truncated to focus on the W_x axis. From this linear model a transfer function from the W_x axis wind, to W_x position $D(s) = X(s)/W_x(s)$ can then be generated. For attitude-based thrust control, this is denoted $D_A(s)$.

$K_{p,xy}$	$K_{p,xy}$	$K_{i,xy}$	$K_{d,xy}$
2	0.09	0.02	0.01
$K_{p,z}$	$K_{p,z}$	$K_{i,z}$	$K_{d,z}$
1	0.2	0.1	0
$K_{p,\theta}$	$K_{p,\theta}$	$K_{i,\theta}$	$K_{d,\theta}$
6.5	0.15	0.05	0.003

Table 1: Gains used for attitude-based thrust control. The final row of gains are for the inner attitude loop, and are preserved with vectored thrust control.

The closed-loop plant for vectored thrust control is then chosen such that the corresponding transfer function $D_V(s)$, has the same magnitude as $D_A(s)$, when evaluated at different frequencies. The closed-loop transfer function $D_V(s)$ is manipulated mainly via the P and PID gains for the horizontal axes (xy).

The magnitude equalisation is undertaken for the following reason. With wind represented by unit white-noise, coloured by a transfer function $Q(s)$, the resulting RMS error in position is given by the \mathcal{H}_2 norm shown in Equation 1.

$$\|D(s)Q(s)\|_2 = \sqrt{\frac{1}{2\pi} \int_{-\infty}^{\infty} |D(j\omega)Q(j\omega)|^2 d\omega} \quad (1)$$

Hence by ensuring $|D_V(j\omega)| \cong |D_A(j\omega)|$, the position performance between the two actuation methods can be preserved, after which actuation can be compared. This is similar in the approach taken in [16], but applied to a simpler controller, in the context of disturbance rejection.

Using the gains generated, insight is gained into the actuation usage by first looking at the PWM, and its variation with frequency in the linear model. In particular, $p(\omega)$ in Equ-

tion 2 represents the average standard deviation in PWM under a sinusoidal unit wind input, at a given frequency.

$$p(\omega) = \frac{1}{8\sqrt{2}} \sum_{i=1}^8 |V_i(j\omega)| \quad : \quad V_i(s) = \chi_i(s)/W_x(s) \quad (2)$$

To further evaluate the relative performance of the two station-keeping methods, both systems are then simulated with the corresponding gains.

3.4 Simulation Description

For simulation tests of the plant, the non-linear model referenced above was used. However, it was augmented to more accurately represent the real system. This involved replacing the continuous attitude controller, with a discrete time version. Also included was a sensor model with the PX4 Extended Kalman Filter (EKF), and the designed closed-loop controller used for position stabilisation. The wind trajectories used as an input to the system are generated from Turbsim. The profiles used are the same as those used in [9]. The spectrum of the wind for two axes is shown in Figure 5.

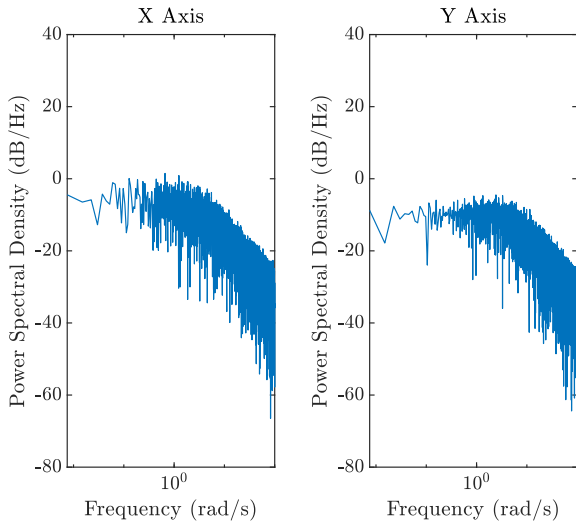


Figure 5: Spectrum of wind speed in the X and Y axes (with mean value removed). Note that the dominant frequencies are below 1Hz. Also, the Z axis is omitted here, but it's spectrum is similar to that in the second.

In order to compare actuation methods in simulation, metrics are generated from measured data. First, RMS position error, from [9], is used and it is given in Equation 3.

$$\sigma_\xi = \sqrt{\frac{1}{M} \sum_{m=1}^M \|\xi_{des,m} - \xi_m\|^2} \quad (3)$$

In Equation 3, $\xi_m \in \mathbf{R}^3$ denotes the position vector each time step m . Meanwhile, $\xi_{des,m}$ denotes the reference position, which is zero at all time steps.

To measure actuator usage, the average motor PWM standard deviation is used, given in Equation 4, from [9].

$$\bar{\sigma}_\chi = \frac{1}{N} \sum_{i=1}^N \sqrt{\frac{1}{M} \sum_{m=1}^M (\chi_{i,m} - \bar{\chi}_i)^2} \quad (4)$$

In Equation 4, χ_i is the PWM of motor i . $\bar{\chi}_i$ denotes the mean PWM of a motor. In both equations M denotes the total number of samples available from simulation.

4 RESULTS

After tuning, the response in Figure 6 is seen, from wind to position, which is clearly matched. The resulting gains for vectored thrust control are shown in Table 2.

$K_{p,xy}$	$K_{p,xy}$	$K_{i,xy}$	$K_{d,xy}$
1.7	0.08	0.02	0
$K_{p,z}$	$K_{p,z}$	$K_{i,z}$	$K_{d,z}$
1	0.2	0.1	0

Table 2: Gains used for vectored thrust control.

The plot of $p(\omega)$ is then shown in Figure 7. It is clearly seen that for most frequencies, the vectored thrust plant will have higher actuator usage (as measured by PWM variation). It is only in the higher frequencies, that vectored thrust has lower actuator usage. This is due to the fact that in this region the disturbances are outside the range of effective frequencies for attitude-based thrust, but still below the bandwidth of vectored thrust. This indicates that despite vectored thrust's superior bandwidth, in most frequencies, it will be less efficient than attitude-based thrust. This further confirms the results from [9] in a closed-loop context.

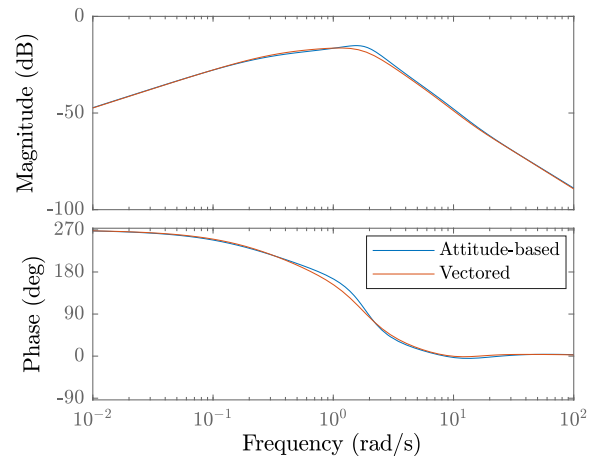


Figure 6: Bode plot from wind to position for the two actuation modes.

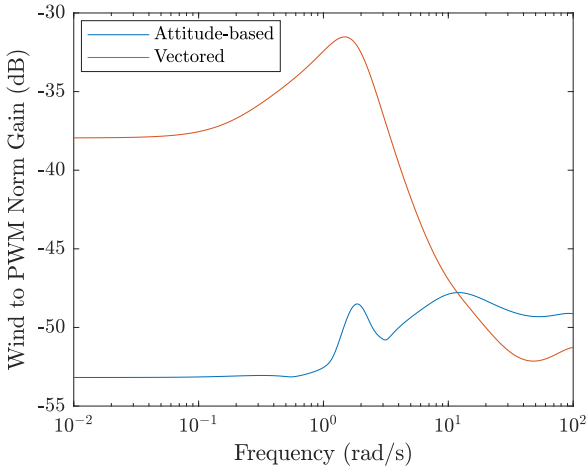


Figure 7: Variation with frequency of the PWM usage, for the two actuation modes.

When these control gains are then simulated, the performance is as described in Table 3.

	$\sigma_{\xi}(mm)$	$\bar{\sigma}_{\chi}$
Attitude-based thrust	66	0.0125
Vectored thrust	66	0.0271

Table 3: Performance parameters for the two tuned plants.

The relative performance of the controllers shown in Table 3 is highly intuitive, as the dominant frequencies in the wind, as seen in Figure 5, mostly overlap with the regions where attitude-based thrust uses much less PWM.

5 DISCUSSION OF CONTROL AGGRESSIVITY

The results in Section 4 correspond to moderate performance. However, also of interest, is how the relative performance of these two actuation methods changes as more aggressive tuning is approached. This is explored here in a linear context via an optimal control problem.

For each actuation method, a linear plant is available. For the linear plant, the position and speed loop controller gains are then optimised to minimise the response of the plant to wind. This is done by minimising the \mathcal{H}_2 norm of the transfer function $D(s)$ for each actuation method. This is evaluated under different constraints on PWM, described in Equation 5.

$$\|\chi_i(s)/W_x(s)\|_2 \leq a(\min(1 - \chi_i^*, \chi_i^*)) \quad \forall i \in \{1, 2, 3, 4\} \quad (5)$$

In Equation 5 the limit on each rotor is scaled according to its distance from saturation at trim. The parameter a then allows the conservativeness to be modified, with higher values corresponding to a more lenient constraint, and a more aggressive controller. In this equation, it should be noted that only the

first 4 motors are used in the constraint. This is because this optimisation focuses on X-axis control, and so symmetry is expected between the motors on each side of the craft.

Control optimisation is undertaken using the 'Systune' tool from MATLAB, which uses optimisation methods discussed in [26]. Ultimately, the optimisation gives results shown in Figure 8, with the a value on the horizontal axis. It can clearly be seen here that for more conservative controllers, the vectored thrust based control performs worse. In this case, under the same actuator usage constraint, vectored thrust has worse position performance. However, under aggressive control, attitude-based thrust control reaches a hard limit.

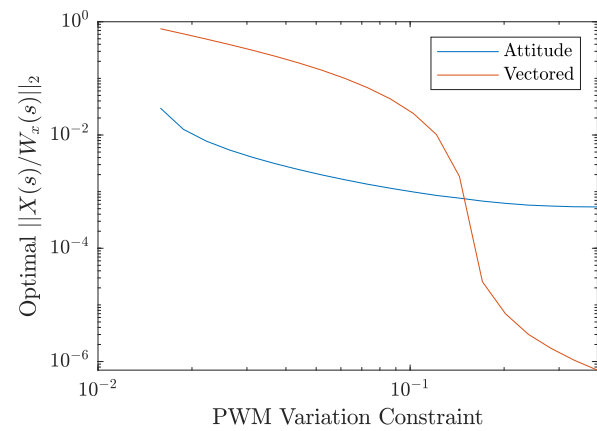


Figure 8: Variation in Optimal Norm, with actuation constraint, for the two actuation modes.

In general, the hard limit reached by attitude-based thrust can best be explained by looking at the pole-zero maps for $X(s)/F_{.,x}(s)$, shown in Figure 9.

It is observed in Figure 9 that the attitude-based thrust plant has zeros close to the imaginary axis. Ultimately this results in poor response of the system to actuation at this frequency, and the limit in attitude-based thrust is likely due to impossibly high levels of actuation which are required to effectively actuate this frequency notch.

This notch arises due to the fact that torque commands in the multirotor mixer (taken from [9]) are imperfect, and produce vectored thrust as a side effect. Whilst this could be fixed by changing coefficients, this mixer *leakage*, will inevitably occur with any linear multirotor mixer, as the operating point changes.

The vectored thrust leakage causes these zero issues, as when attitude-based thrust is used, a torque can only create translation through an angle change. As a result the acceleration due to attitude changes can roughly be described in Equation 6, where $\tau(s)$ represents the pitching torque.

$$s^2 X(s) \cong \frac{\alpha}{s^2} \tau(s) \quad (6)$$

http://www.imavs.org/

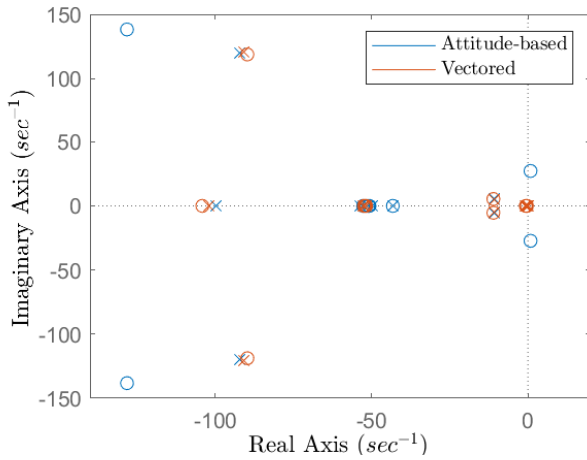


Figure 9: Pole Zero maps for $X(s)/F_x(s)$, with the two modes of actuation.

However, the leaked force will generate a force, as described in Equation 7.

$$s^2 X(s) \cong \frac{1}{m} \alpha_l \tau(s) \quad (7)$$

In Equation 7, α_l is a factor, describing how the leaked force is related to the applied torque. As a result, if α and α_l are of the same sign, the acceleration generated by the leaked force will be out of phase with the intended acceleration from the original torque command. When these are of the same magnitude, notches appear in the frequency response, which in turn creates problematic plant properties.

However, in tuning the controllers in simulation, this difference hasn't manifested in a significant manner. This is likely due to limitations in sensors and actuators, such as saturation and delay, which dominate over plant effects. For example, the simulation model of the extended Kalman filter is based on EKF, rather than the newer EKF2, available in the PX4 firmware [9]. Fixes to this may reveal aggressive tuning to be an area worth exploring.

6 CONCLUSION

This work has focused on identifying differences in how simple P-PID controllers can be tuned for wind disturbance rejection when various actuation methods are used on a fully-actuated octorotor. It has been found that by virtue of its less efficient force generation, vectored thrust tends to yield higher actuator usage when providing the same wind disturbance rejection performance, despite its high bandwidth. However, preliminary studies have shown that when the goal is a more aggressive tuning, attitude-based thrust control may be limited by its dynamics. Possible future work includes investigating comparison with more involved control methods. This work can also be extended to an experimental study.

ACKNOWLEDGEMENTS

The research reported was conducted as part of “Enabling unmanned aerial vehicles (drones) to use tools in complex dynamic environments UOCX2104”, funded by the New Zealand Ministry of Business, Innovation and Employment.

REFERENCES

- [1] Victoria Gonzalez-Dugo, P. Zarco-Tejada, E. Nicolás, Pedro Antonio Nortes, J. J. Alarcón, Diego S. Intrigliolo, and E.J.P.A. Fereres. Using high resolution UAV thermal imagery to assess the variability in the water status of five fruit tree species within a commercial orchard. *Precision Agriculture*, 14:660–678, 2013.
- [2] Ruimin Ke, Zhibin Li, Sung Kim, John Ash, Zhiyong Cui, and Yinhai Wang. Real-time bidirectional traffic flow parameter estimation from aerial videos. *IEEE Transactions on Intelligent Transportation Systems*, 18(4):890–901, 2017.
- [3] Chuang Deng, Shengwei Wang, Zhi Huang, Zhongfu Tan, and Junyong Liu. Unmanned aerial vehicles for power line inspection: A cooperative way in platforms and communications. *J. Commun.*, 9(9):687–692, 2014.
- [4] Hazim Shakhathreh, Ahmad H. Sawalmeh, Ala Al-Fuqaha, Zuocho Dou, Eyad Almaita, Issa Khalil, Noor Shamsiah Othman, Abdallah Khreishah, and Mohsen Guizani. Unmanned aerial vehicles (UAVs): A survey on civil applications and key research challenges. *IEEE Access*, 7:48572–48634, 2019.
- [5] James R. Kutia, Karl A. Stol, and Weiliang Xu. Aerial manipulator interactions with trees for canopy sampling. *IEEE/ASME transactions on mechatronics*, 23(4):1740–1749, 2018.
- [6] Peter Zheng, Xinkai Tan, Basaran Bahadir Kocer, Erdeng Yang, and Mirko Kovac. TiltDrone: A fully-actuated tilting quadrotor platform. *IEEE Robotics and Automation Letters*, 5(4):6845–6852, 2020.
- [7] Jorge M. Arizaga, Herman Castañeda, and Pedro Castillo. Adaptive control for a tilted-motors hexacopter UAS flying on a perturbed environment. In *International Conference on Unmanned Aircraft Systems (ICUAS)*, pages 171–177, 2019.
- [8] Markus Ryll, Davide Bicego, and Antonio Franchi. Modeling and control of FAST-hex: a fully-actuated by synchronized-tilting hexarotor. In *IEEE/RSJ International Conference on Intelligent Robots and Systems (IROS)*, pages 1689–1694, 2016.
- [9] Jérémie Xavier Joseph Bannwarth. *Aerodynamic modelling and wind disturbance rejection of multirotor unmanned aerial vehicles*. PhD thesis, The University of Auckland, 2021.

- [10] Shi Lu, Armando Rodriguez, Konstantinos Tsakalis, and Yan Chen. Design and characteristics of a new transformable UAV with both coplanar and omnidirectional features. In *International Conference on Unmanned Aircraft Systems (ICUAS)*, pages 831–838, 2022.
- [11] Guangying Jiang and Richard Voyles. A nonparallel hexrotor UAV with faster response to disturbances for precision position keeping. In *IEEE International Symposium on Safety, Security, and Rescue Robotics*, pages 1–5, 2014.
- [12] Dario Brescianini and Raffaello D’Andrea. An omnidirectional multirotor vehicle. *Mechatronics*, 55:76–93, 2018.
- [13] Mahathi Bhargavapuri, Jay Patrikar, Soumya Ranjan Sahoo, and Mangal Kothari. A low-cost tilt-augmented quadrotor helicopter : modeling and control. In *International Conference on Unmanned Aircraft Systems (ICUAS)*, pages 186–194, 2018.
- [14] Michelangelo Nigro, Francesco Pierri, and Fabrizio Caccavale. Preliminary design, modeling and control of a fully actuated quadrotor UAV. In *International Conference on Unmanned Aircraft Systems (ICUAS)*, pages 1108–1116. IEEE, 2019.
- [15] Runit Kumar, Shubham R. Agarwal, and Manish Kumar. Modeling and control of a tethered tilt-rotor quadcopter with atmospheric wind model. *IFAC-PapersOnLine*, 54(20):463–468, 2021.
- [16] Murray L Ireland, Aldo Vargas, and David Anderson. A comparison of closed-loop performance of multirotor configurations using non-linear dynamic inversion control. *Aerospace*, 2(2):325–352, 2015.
- [17] G Bressan, D Invernizzi, S Panza, M Lovera, et al. Attitude control of multirotor uavs: cascade P/PID vs PI-like architecture. In *5th CEAS Specialist Conference on Guidance, Navigation and Control-EuroGNC*, pages 1–20, 2019.
- [18] Shilin Yi. *Modeling and control of an over-actuated quadrotor manipulator with four tiltable rotors*. PhD thesis, Okayama University, 2022.
- [19] Jorge A. Ricardo Jr and Davi A. Santos. Smooth second-order sliding mode control for fully actuated multirotor aerial vehicles. *ISA Transactions*, 129:169–178, 2022.
- [20] Maximilian Brunner, Karen Bodie, Mina Kamel, Michael Pantic, Weixuan Zhang, Juan Nieto, and Roland Siegwart. Trajectory tracking nonlinear model predictive control for an overactuated MAV. In *IEEE International Conference on Robotics and Automation (ICRA)*, pages 5342–5348, 2020.
- [21] Panfeng Shu, Feng Li, Junjie Zhao, and Masahiro Oya. Robust adaptive control for a novel fully-actuated octocopter uav with wind disturbance. *Journal of Intelligent & Robotic Systems*, 103(6):1–17, 2021.
- [22] Tomoki Anzai, Moju Zhao, Masaki Murooka, Fan Shi, Kei Okada, and Masayuki Inaba. Design, modeling and control of fully actuated 2D transformable aerial robot with 1 DoF thrust vectorable link module. In *IEEE/RSJ International Conference on Intelligent Robots and Systems (IROS)*, pages 2820–2826. IEEE, 2019.
- [23] Guangying Jiang, Richard M Voyles, and Jae Jung Choi. Precision fully-actuated UAV for visual and physical inspection of structures for nuclear decommissioning and search and rescue. In *IEEE International Symposium on Safety, Security, and Rescue Robotics (SSRR)*, pages 1–7, 2018.
- [24] Z. J. Chen, K. A. Stol, and P. J. Richards. Preliminary design of multirotor UAVs with tilted-rotors for improved disturbance rejection capability. *Aerospace Science and Technology*, 92:635–643, 2019.
- [25] C. Probine, D. Yang, K. A. Stol, and N. Kay. Model predictive control on a fully-actuated octocopter for wind disturbance rejection. In *International Micro Aerial Vehicle Conference (IMAV)*, 2023.
- [26] Pierre Apkarian, Pascal Gahinet, and Craig Buhr. Multi-model, multi-objective tuning of fixed-structure controllers. In *European Control Conference (ECC)*, pages 856–861, 2014.